Testing atomic collision theory with the two-photon continuum of astrophysical nebulae

F. Guzmán,[1][*] N. R. Badnell,[2] M. Chatzikos,[1] P. A. M. van Hoof,[3] R. J. R. Williams[4] and G. J. Ferland[1]

[1]*Department of Physics and Astronomy, University of Kentucky, Lexington, KY 40506, USA*
[2]*Department of Physics, University of Strathclyde, Glasgow G4 0NG, UK*
[3]*Royal Observatory of Belgium, Ringlaan 3, B-1180 Brussels, Belgium*
[4]*AWE plc, Aldermaston, Reading RG7 4PR, UK*

ABSTRACT

Accurate rates for energy-degenerate *l*-changing collisions are needed to determine cosmological abundances and recombination. There are now several competing theories for the treatment of this process, and it is not possible to test these experimentally. We show that the H I two-photon continuum produced by astrophysical nebulae is strongly affected by *l*-changing collisions. We perform an analysis of the different underlying atomic processes and simulate the recombination and two-photon spectrum of a nebula containing H and He. We provide an extended set of effective recombination coefficients and updated *l*-changing $2s - 2p$ transition rates using several competing theories. In principle, accurate astronomical observations could determine which theory is correct.

Key words: atomic data – atomic processes – H II regions – planetary nebulae: general – cosmic background radiation – cosmology: observations.

1 MOTIVATION

Optical recombination lines (ORL) are produced from recombination of ions followed by cascades from highly excited recombined levels. Theoretical emissivities of these lines should be known with high accuracy, and observations of such lines in nebulae provide valuable and accurate information on their composition, temperature and density. This is summarized in the textbook of Osterbrock & Ferland (2006), while Schirmer (2016) applies this theory to spectral simulations.

Although many processes contribute to the formation of these lines, recently attention has been brought to *l*-changing collisions. These act to redistribute the populations within an *n*-shell and so change the subsequent cascade to lower levels. Intra *n*-shell *l*-levels are energy degenerate for hydrogenic systems, so the orbiting electron changes its angular momentum with no energy change. This is caused by a long range Stark interaction with the electric field of the projectile. Due to this peculiarity, slow high-mass projectiles are favoured over electrons.

There are now several competing theories for how *l*-changing collisions occur, as summarized in our previous work (Guzmán et al. 2016, 2017, hereafter P1 and P2). These have an important effect on recombination line intensities, as shown in P1 and P2. In addition, *l*-mixing collisions in relatively low *n*-shells play an important role in producing cosmological recombination radiation (CRR; Chluba, Vasil & Dursi 2010). In fact, Ly*α* and two-photon emissivities are the two bottlenecks at different redshifts: Ly*α* at $z > 1300$, and two photons at lower redshift during the recombination epoch. Chluba & Sunyaev (2006) show that an accurate treatment of *l*-mixing collisions, and the 2*s* and 2*p* populations is needed to predict the cosmic microwave background to a precision of ∼0.1 per cent. These processes have a similar effect on helium recombination lines, which introduces uncertainties in measurements of the primordial helium abundance (Porter et al. 2009).

It is not possible to experimentally determine which of the *l*-changing theories is correct. Measurements of *l*-changing rates have been done for high-*n* and low-*l* Na atoms colliding with different ions (see e.g. MacAdam, Crosby & Rolfes 1980; MacAdam, Rolfes & Crosby 1981; MacAdam et al. 1987; Sun & MacAdam 1993; Irby et al. 1995), but these levels are not hydrogenic. We know of no experimental measurements of energy degenerate *l*-changing rates or cross-sections.

In this paper, we outline an astronomical observation, which, in principle, would make it possible to discriminate between competing *l*-changing theories. The H I two-photon continuum, the subject of this paper, is sensitive to the *l*-changing theory since the population of 2*s*, the level producing the two-photon continuum, is affected by both cascades from higher levels, and the rate of collisions

[*] E-mail: francisco.guzman@uky.edu

Table 1. Comparison of rate coefficients ($cm^3 s^{-1}$) by the different theoretical *l*-changing collision theories for $n = 2$ and at different temperatures. PS-M: modified method from P64 (see P2); QM: Vrinceanu & Flannery (2001); SC: Vrinceanu & Flannery (2001); SSC: Simplified SC method of Vrinceanu et al. (2012); AGN: results from table 4.10 of Osterbrock & Ferland (2006) obtained using PS64.

		$T_H = 100$ K	$T_H = 1000$ K	$T_H = 5000$ K	$T_H = 10\,000$ K	$T_H = 15\,000$ K	$T_H = 20\,000$ K
$2s\,^2S \rightarrow 2p\,^2P^0_{1/2}$	QM	1.73e-4	3.55e-4	2.92e-4	2.49e-4	2.24e-4	2.07e-4
	PS-M	1.55e-4	3.58e-4	2.96e-4	2.52e-4	2.26e-4	2.09e-4
	SC	1.53e-3	4.82e-4	2.15e-4	1.53e-4	1.25e-4	1.08e-4
	SSC	4.18e-4	1.32e-4	5.92e-5	4.18e-5	3.42e-5	2.96e-5
	AGN (PS64)	–	–	–	2.51e-4	–	2.08e-4
$2s\,^2S \rightarrow 2p\,^2P^0_{3/2}$	QM	4.92e-6	1.17e-4	2.24e-4	2.30e-4	2.26e-4	2.20e-4
	PS-M	4.56e-6	1.06e-4	2.24e-4	2.34e-4	2.28e-4	2.22e-4
	SC	2.88e-3	9.11e-4	4.08e-4	2.88e-4	2.35e-4	2.04e-4
	SSC	8.36e-4	2.64e-4	1.18e-4	8.36e-5	6.84e-4	5.92e-5
	AGN (PS64)	–	–	–	2.23e-4	–	2.19e-4

between 2*s* and 2*p*. Section 2 examines collision rates at various temperatures and densities. In Section 3, emissivities are obtained using the different collisional rates. We present a method to distinguish observationally between the different theoretical methods, provided that accurate kinetic temperatures are known. Alternatively, if the modified Pengelly & Seaton (1964) rate coefficients presented in P2 are accepted, the intensity of the two-photon continuum can be used as a diagnostic of the temperature. A discussion of these results is given in Section 4, and a summary is given in Section 5.

2 DETERMINATION OF $n = 2$ POPULATIONS AND THE TWO-PHOTON SPECTRUM

The H I two-photon continuum emission originates from the transition $2s - 1s$, which is strictly forbidden for single-photon processes. As the total energy of the two photons is conserved, the energy of one photon can take any value $0 < E < \Delta E_{1s2s}$. The two-photon process has a spontaneous transition probability that depends on the frequency of the photons $A^{2v,H}_{2s1s,v}(v)$ (Spitzer & Greenstein 1951; Nussbaumer & Schmutz 1984).

In addition to two-photon spontaneous decays to 1*s*, the metastable level 2*s* can also be collisionally excited to 2*p* by *l*-changing transitions and to np ($n > 2$) by *n*-changing transitions, although the *l*-changing collisions are by far the fastest process. Such collisions populate 2*p* that then decays to 1*s* by a dipole transition producing Lyα. Likewise, when the Lyα line is extremely optically thick in Case B (Brown & Mathews 1970), *l*-changing collisions finally transfer the 2*p* population to 2*s*. As a result, the 2*s* population and the two-photon emissivity will have a strong density dependence.

The rate coefficients for the $2s - 2p$ *l*-changing transition are tabulated in Table 1 for the competing available theories. The quantum mechanical (QM) approach of Vrinceanu & Flannery (2001) and the Bethe–Born approach of Pengelly & Seaton (1964, PS64) need a cut-off to eliminate the divergence of the probabilities at high impact parameters. These cut-offs depend either on collective effects, such as the plasma Debye length, or the lifetime of the initial state (P1).[1] This, together with the numerical difficulties of the QM calculations at high *n*-shells ($n > 60$), due to the lack of precision introduced by instabilities caused by the oscillatory behaviour of the hypergeometrical functions needed to compute the cross-sections,

led Vrinceanu & Flannery (2001) to propose a semiclassical (SC) alternative approach. Both QM and SC methods are summarized again in Vrinceanu, Onofrio & Sadeghpour (2012).

P1 shows that the results of the SC approach disagree with the predictions of both the QM and the PS64 results, mainly because it lacks a complete description of the collision at a high impact parameter, a point made by Storey & Sochi (2015). Indeed, in Table 1, the QM and modified PS64 (PS-M) approaches give very similar results, which disagree by a factor of ~ 2 with the SC results. This factor increases up to an order of magnitude for lower temperatures and up to a factor of ~ 6 at higher *nl*. The QM and PS64 results coincide closely with table 4.10 of Osterbrock & Ferland (2006), which is called active galactic nuclei (AGN) in Table 1, and was obtained using PS64. A further simplification that we have called the simplified semiclassical (SSC) method to distinguish it from the original SC approach is done by Vrinceanu et al. (2012), where the scaled angular moment, l/n, is taken to be continuous. Since $n = 2$ is such an extreme case, where l/n is highly discrete, it is not surprising that this approximation does not work well and results are slightly worse. This approximation makes sense only at sufficiently high quantum number *n*, where the SC predictions may be approximated by the SSC method to an analytic formula, which is easy to implement.

The rate coefficients in Table 1 decrease with temperature as the Stark *l*-mixing produced by the charged projectile is less effective at increasing projectile velocities. As seen in P1, at very low temperatures, the lifetime cut-off decreases the effectiveness of the collision for QM and PS-M. The SC and SSC methods do not account for these effects and the rate coefficients continue increasing linearly at low temperatures.

The rates in Table 1, together with the other collisional and radiative processes, are combined with effective recombination coefficients to predict the 2*s* population and thus the two-photon continuum emissivity. In equilibrium, and in absence of charge exchange, the population of the hydrogen *nl*-level, n_{nl}, is given by

---

[1] This can introduce a dependence on the effective rates on density. However, for the transitions considered in Table 1, the lifetime cut-off dominates at the astrophysical low densities considered.

$$n_e n_p \alpha^{eff}_{nl} + \sum_{n'l' \neq nl} n_e n_{n'l'} q_e \left(n'l' \rightarrow nl \right) + \sum_{l' \neq l} n_p n_{nl'} q_p \left(nl' \rightarrow nl \right)$$

$$= n_{nl} \left[\sum_{n'l' \neq nl} n_e q_e \left(nl \rightarrow n'l' \right) + \sum_{l' \neq l} n_p q_p \left(nl \rightarrow nl' \right) \right.$$

$$\left. + n_e S_{nl} + \sum_{n'l' < nl} A_{nl \rightarrow n'l'} \right], \tag{1}$$

Table 2. Comparison of effective recombination coefficients (10^{-13} cm^{3}s^{-1}) to **2s** and **2p** calculated for Case A and Case B using QM *l*-changing collisions at different temperatures and densities. P64: Results from Pengelly (1964) are quoted in Osterbrock & Ferland (2006).

			$T = 100$ K	$T = 1000$ K	$T = 5000$ K	$T = 10\,000$ K	$T = 15\,000$ K	$T = 20\,000$ K
Case A	2s	$n_e = n_H = 10^2$cm^{-3}	4.16	1.15	0.475	0.318	0.249	0.208
		$n_e = n_H = 10^4$cm^{-3}	5.77	1.22	0.481	0.320	0.250	0.209
		$n_e = n_H = 10^6$cm^{-3}	14.9	1.45	0.503	0.328	0.254	0.211
		P64($n_e = n_H \to 0$)	–	–	0.475	0.318	–	0.208
	2p	$n_e = n_H = 10^2$cm^{-3}	56.2	10.8	3.02	1.65	1.14	0.869
		$n_e = n_H = 10^4$cm^{-3}	65.3	10.6	2.98	1.64	1.13	0.864
		$n_e = n_H = 10^6$cm^{-3}	123	10.9	2.92	1.61	1.11	0.853
		P64($n_e = n_H \to 0$)	–	–	3.07	1.67	–	0.877
Case B	2s	$n_e = n_H = 10^2$cm^{-3}	14.1	3.54	1.33	0.835	0.625	0.505
		$n_e = n_H = 10^4$cm^{-3}	20.4	3.76	1.34	0.838	0.626	0.505
		$n_e = n_H = 10^6$cm^{-3}	53.3	4.50	1.39	0.850	0.630	0.507
		P64($n_e = n_H \to 0$)	–	–	1.33	0.837	–	0.507
	2p	$n_e = n_H = 10^2$cm^{-3}	59.0	11.2	3.17	1.74	1.20	0.920
		$n_e = n_H = 10^4$cm^{-3}	72.3	11.3	3.15	1.74	1.20	0.918
		$n_e = n_H = 10^6$cm^{-3}	152	12.2	3.18	1.74	1.21	0.922
		P64($n_e = n_H \to 0$)	–	–	3.21	1.76	–	0.927

where $A_{nl \to n'l'}$ are the Einstein coefficients for the spontaneous $nl \to n'l'$ decay; n_e, n_p are the electron and proton density, respectively, $q_e(n'l' \to nl)$ is the collisional transition rate (by electron impact) from the $n'l'$-shell to the nl-shell, $q_p(nl' \to nl)$ is the intra n-shell collisional transition rate (by proton impact) from the l'-subshell to the l-subshell, S_{nl} are the ionization rate coefficients and α_{nl}^{eff} are the effective recombination coefficients to the nl shell. Proton n-changing collisions and electron l-changing collisions are neglected. The effective recombination coefficients are given by

$$n_e n_p \alpha_{nl}^{\text{eff}} = n_e n_p \alpha_{nl}^{\text{rad}} + n_e^2 n_p \alpha_{nl}^{3b} + \sum_{n'l' > nl} n_{n'l'} A_{n'l' \to nl}, \quad (2)$$

where α_{nl}^{rad} are the radiative recombination rate coefficients (in units of cm^{3}s^{-1}) and α_{nl}^{3b} three-body recombination rate coefficients (in units of cm^{6}s^{-1}). α_{nl}^{eff} includes direct recombination to the nl-shell plus decays from upper levels that have already recombined and/or suffered collisions.

We have used the development version of the spectral code CLOUDY, which is most recently described by Ferland et al. (2013), to calculate the α_{nl}^{eff}. The calculated coefficients are given in Table 2 and in Fig. 1 for different temperatures and densities where the QM method has been used. Case A and Case B H I line formation have been assumed (Osterbrock & Ferland 2006). Case B systematically produces larger recombination line emissivities since Ly lines are re-absorbed and converted into Balmer lines (Baker & Menzel 1938). At temperatures $T > 10^3$ K, the effective coefficients depend weakly on the density and agree with the collisionless work of Pengelly (1964). This is because radiative decays are faster than collisions at these densities. In Table 2 and the top graph of Fig. 1, it is seen that the density dependence becomes strong at low temperatures $T < 10^3$ K. High n-shell l-changing collisions are more efficient at these temperatures, producing a more effective l-mixing. This affects the cascade towards the low levels and changes the populations. Different l-changing methods are also compared in the bottom graph of Fig. 1 and no differences are found between them. We conclude that the differences between l-changing methods have a small influence on effective recombination coefficients even at low
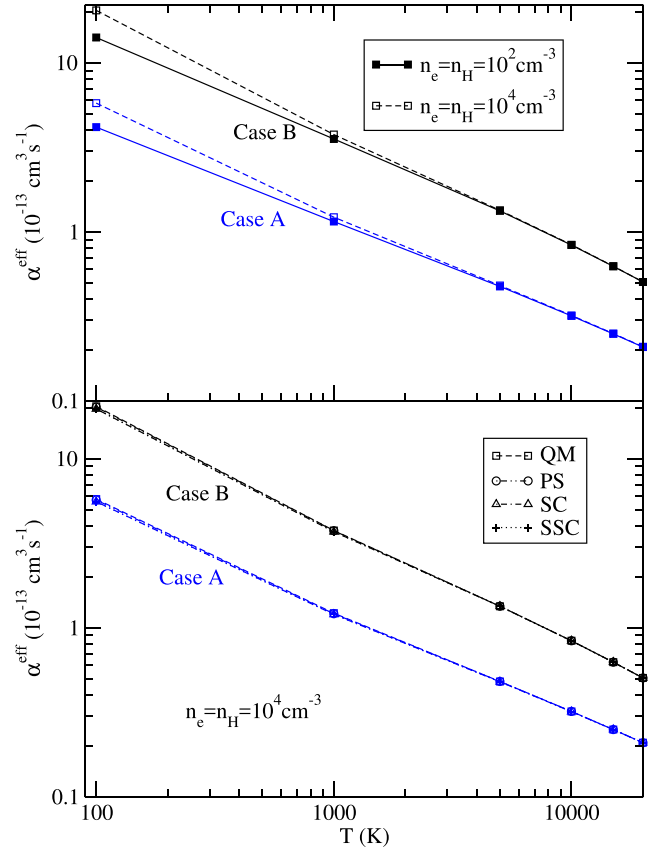

Figure 1. Top panel: effective recombination coefficients to 2s using QM *l*-changing method for Case A (blue) and Case B (black) and different densities. Bottom panel: comparison of different *l*-changing methods for effective coefficients for Case A (blue) and Case B (black).

temperatures. However, once the metastable 2s level is reached, *l*-changing collisions strongly influence the $2s - 2p$ populations, and produce measurable differences in the two-photon emission.

3 DEPENDENCE OF TWO-PHOTON CONTINUUM ON TEMPERATURE AND DENSITY

Using the different theoretical approaches, we run simulations with the spectral code CLOUDY and calculated emissivities for a layer of H/He gas at constant temperature, illuminated by a mono-energetic 'laser' radiation of 1.1 Ryd, enough to ionize hydrogen but not to fluoresce any H I lines. This is done in order to model an optically thick environment that keeps with Case B assumptions (Baker & Menzel 1938). For simplicity, we assume that the heavy elements have negligible abundances, while the He/H abundance ratio is taken to be 10 per cent, similar to cosmic abundances. The ionization parameter, which is the ratio of ionizing photon to hydrogen atom densities, is $U = 0.1$. The chosen temperature and density of the hydrogen atoms is $T_e = 15\,000$ K and $n_H = 10^4 \text{cm}^{-3}$. The electron density is calculated consistently depending on the He ionization degree (H is fully ionized while He is atomic due to the low energy of the laser). If He atoms are singly ionized, then the electron density would be 10 per cent higher than n_H. Our proposed test compares Case B predictions with observations of a nebula. It is possible that such processes as continuum pumping of the Lyman lines, or their escape from the cloud, would mitigate the Case B assumption and change the resulting emission. As a test, we recomputed a standard model of a young planetary nebula, including our large H I model. The model is our 'pn_paris' in the CLOUDY test suite. It was a standard model in the 1984 Meudon meeting (Péquignot 1986), and has been included in subsequent photoionization workshops (Péquignot et al. 2001; Ferland et al. 2016). We found that the H I lines agreed with the Hummer & Storey (1987) Case B predictions to a small fraction of a per cent for H I lines, ∼0.3 per cent. Our pure Case B calculations agree with the Hummer & Storey (1987) ones to about this difference, due to change in the atomic data over the past few decades. In view of that, we can rely on Case B approximation as highly accurate.

The ratio of the total integrated two-photon continuum intensity relative to Case B Hβ is presented in Fig. 2 for the different *l*-changing theories. The relative two-photon flux decays exponentially for intermediate densities since *l*-changing collisions depopulate the 2*s* levels by $2s - 2p$ transitions before they can radiate. At these densities, the Hβ emissivity $4\pi j(H\beta)/n_e n_p$ does not vary by much. In Fig. 2, the lower *l*-changing rates from the SSC approach have the effect of maintaining a higher population in the 2*s* level at intermediate densities, producing a higher two-photon flux. However, as it has been pointed out in Section 2, this approximation is probably wrong for low *n*-shells with a highly discrete *l/n* grid. On the other hand, SC calculations give only a slightly higher emissivity than the PS-M and QM calculations, which are indistinguishable from each other. The SC approach usually gives rates that are a factor of ∼6 lower than PS-M and QM (see P1, P2 and Vrinceanu et al. 2012). However, for the transition listed in Table 1, the very similar values of the SC and QM rate coefficients cause the two-photon flux predictions to be similar.

Fig. 2 shows that the two-photon-to-Hβ intensity ratio is strongly affected by both density and collision theory. The two-photon continuum can be detected on the same spectrum as H I Balmer lines so it should be possible to measure this ratio. It may be possible to observationally test which theory is correct by observing the continuum at a wavelength with no contamination from other lines. It is possible to determine the kinetic temperature and gas density from the emission-line spectrum, as described in Osterbrock & Ferland (2006). The instrumental properties and the density of lines would
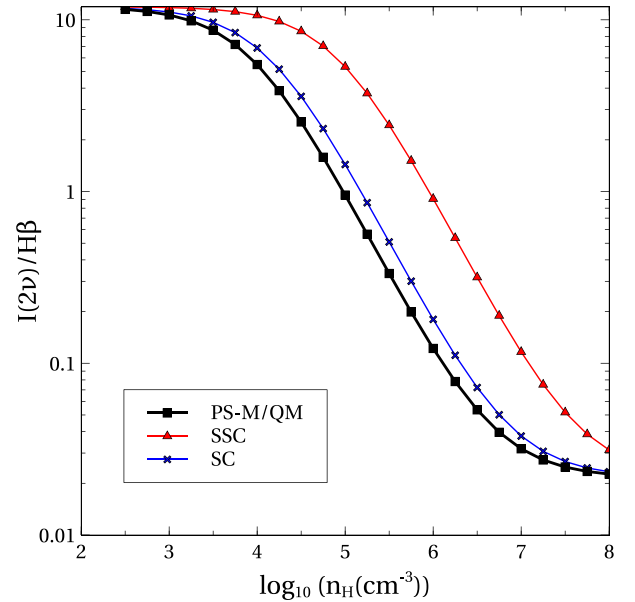

Figure 2. The total integrated two-photon-to-Hβ intensity ratio as a function of hydrogen density. The different lines represent the different theories for the *l*-changing rates.
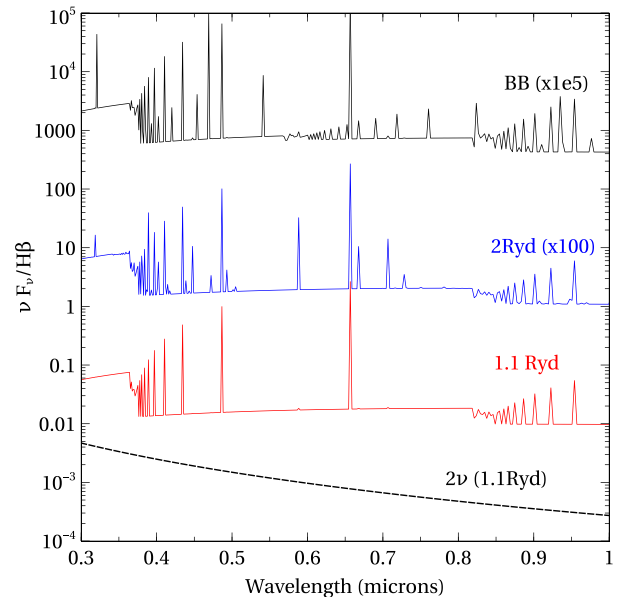

Figure 3. CLOUDY simulations of the emission spectrum of a mono-layer of He and H gas with He/H = 0.1 at 15 000 K and $n_H = 10^4 \text{cm}^{-3}$ illuminated by a 10^5 K BB and two mono-energetic 'laser' radiation fields at 1.1 and 2 Ryd, respectively (see the text). The H I two-photon radiation contribution is shown for the 1.1 Ryd case (dashed line). The incident continuum has been subtracted from the BB spectrum. The 2 Ryd and the BB spectra have been multiplied by 10^2 and 10^5 for clarity.

affect the choice of the specific wavelength range to conduct this test.

Fig. 3 shows the full spectrum normalized to the Hβ flux for our pure H and He cloud. We have carried out photoionization simulations with three different incident radiation fields. The first was a mono-energetic radiation of 1.1 Ryd, which can ionize only H. A second mono-energetic radiation field at 2 Ryd could ionize H
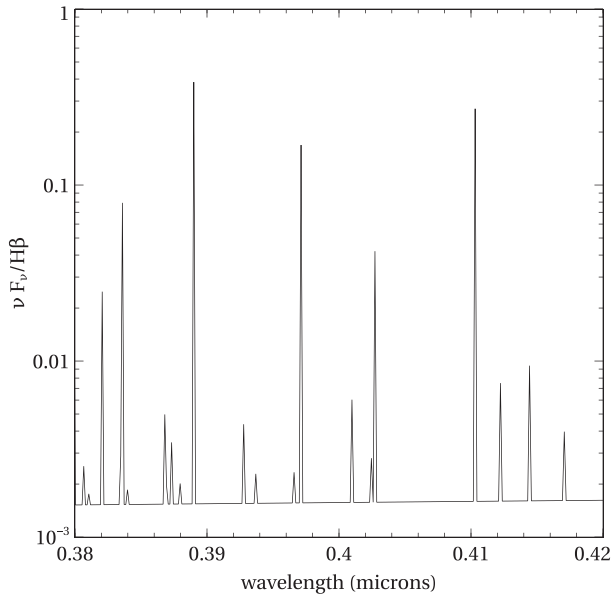
Figure 4. Fine resolution laser 1.1 Ryd spectrum (see Fig. 3).

Figure 5. Simulation of the ratio of selected fluxes to Case B Hβ. Top panel: the total integrated two-photon continuum intensity. Middle panel: the flux at 3900 Å. Bottom panel: BJ. The different colours of the lines represent the different choice of *l*-changing rates: PS-M/QM: black; SC: blue; SSC: red.

and produce He$^+$. Helium ions are heavier than protons and slower at the same temperature. *l*-changing rates with He$^+$ ions will be higher than those produced by protons. However, this contribution is reduced by the much lower abundance of helium atoms. Finally, a blackbody (BB) radiation field with temperature $T_{BB} = 10^5$ K, which can fully ionize both H and He. This is plotted with the 'BB' label and corresponds to a planetary nebula. Again, line fluorescence processes have been excluded. When the incident continuum is bright enough to ionize He, as in the top and middle spectra of Fig. 3, He I recombination lines from $n > 2$ to $2s$ and $2p$ are on the spectrum. Helium is mostly singly ionized when the 2 Ryd radiation is used and double ionized in the case of BB where He II series is also visible. In these two latter cases, the two-photon continuum will be the sum of H and He contributions. In this work, for simplicity, we will take the case of 1.1Ryd radiation that ionizes H only. In our calculations, He I two-photon contribution can be up to an ∼15 per cent for the 2 Ryd radiation case and is less than 0.2 per cent for the 1.1 Ryd radiation case.

It is desirable to use a wavelength that is dominated by the two-photon continuum and clear of emission lines. Regions just longward of the Balmer jump (BJ) would be difficult due to the confluence of the hydrogen Balmer lines. For reference, we have chosen a region around 3900 Å, where no Balmer lines occur (see Fig. 4) and where the two-photon flux is a major contributor to the total continuum (see Fig. 3). This wavelength is in regions where CCD detectors are still efficient. However, due to the smooth behaviour of the two photon continuum, any slight alteration of the selected wavelength will produce the same results.

4 DISCUSSION

The discussion above suggests that it may be possible to observationally test the *l*-changing theory. Fig. 5 shows three emission quantities, all relative to the Case B Hβ. The top panel shows the integrated two-photon continuum emission, the middle shows the total flux at 3900 Å, while the bottom panel shows the flux at the head of the BJ. These are plotted as a function of density and over the range of temperatures found in nebulae. Predictions from
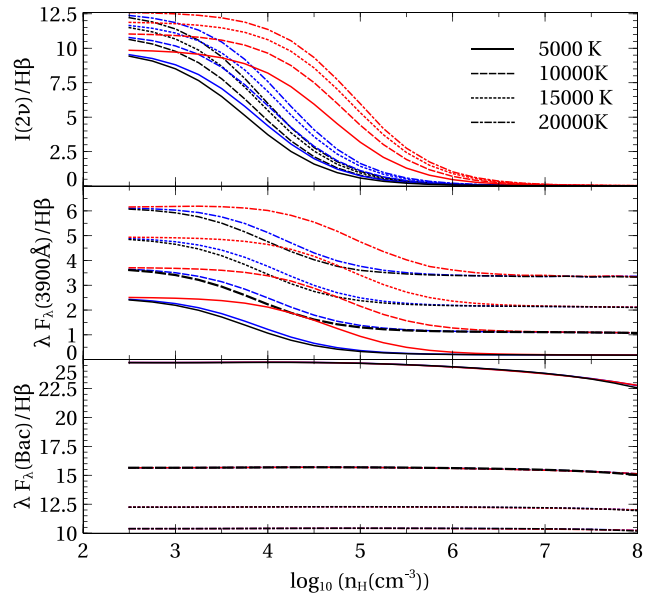
three proposed *l*-changing collision theories are shown. Fig. 5 shows that the biggest differences in the two-photon flux resulting from the various theories are found at densities $n_H \sim 10^4 \text{cm}^{-3}$, where the SSC predictions are a factor of ∼3 greater than the PS-M/QM ones. SC results are ∼10 per cent over PS-M/QM. These densities have been observed in planetary nebulae.

Many nebulae present complex geometries with observations often indicating that density fluctuations are present (Zhang & Liu 2002; Liu 2012; Peimbert & Peimbert 2013). Using different collisionally excited lines (CELs) to measure the density lead typically to a factor of ∼2 uncertainty in the value of the density (Fang & Liu 2011, 2013; Peimbert & Peimbert 2013), although uncertainties can reach much higher values.

An accurate determination of the temperature may be harder to obtain due to the well-known discrepancy between CEL and ORL abundances in planetary nebulae (García-Rojas & Esteban 2007; Peimbert 1967), which can be expressed as temperature variations. Ferland et al. (2016) discuss both this and the suggestion that 'kappa distribution' electrons may be present. Other explanations have been proposed, such as density fluctuations in the nebula (Liu et al. 2000; McNabb et al. 2013) or by the effects of a binary central star (Jones et al. 2016). Our two-photon spectrum should be associated with the ORL temperatures, which can vary by a factor of ∼2 depending on the observed lines. However, it is not unusual to observe much larger discrepancies.

The observational challenge is great, but accurate *l*-changing collisional rates are needed to obtain accurate lines emissivities. As mentioned above, this cannot be done in the laboratory. Such a measurement would be specially desirable and would contribute to our understanding of the basic atomic processes underlying nebular emission.

It should be noted that accurate measurements of both temperature and density are needed to make a decisive test of the various theories.
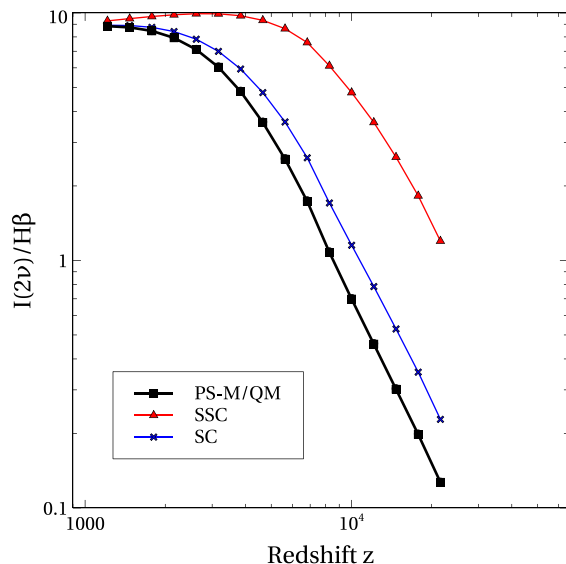
Figure 6. The total integrated two-photon-to-Hβ intensity ratio as a function of z. As in Fig. 2, the different lines represent the different theories for the l-changing rates. Critical density $\rho_c = 8.62 \times 10^{-30}$ g cm^{-3} and $\Omega_b h^2 = 0.022\,30$ (Planck Collaboration XIII 2016).

Finally, it is important to recall here that SSC rates have been used recently in CRR calculations (Glover et al. 2014; Chluba & Ali-Haïmoud 2016), where a high precision of $\sim$0.1 per cent is required (see Section 1). In Fig. 6, we show the two-photon total emission from steady-state simulations due to the recombination of ionized hydrogen at the temperature and density conditions of redshifts previous to the recombination epoch. Hydrogen atoms are ionized using a 'laser' source of 1.1 Ry, as described in Section 3. These results suggest that significant errors in the two-photon emission can emerge by using the SSC approximation. However, l-changing rate coefficients may not be relevant at $z < 1000$ due to the predominance of radiative processes.

5 SUMMARY AND CONCLUSIONS

The discrepancies between the various l-changing collisional theories have an impact on accurate spectroscopic diagnostics of astrophysical plasmas. This paper examines their impact on the two-photon continuum in nebulae. We provide updated $2s - 2p$ l-changing rate coefficients and H I $n = 2$ effective recombination coefficients. These last are only slightly affected by the various l-changing collision theories at moderate to high temperatures. However, these differences of 1 per cent could compromise tests of cosmological models (Chluba & Sunyaev 2006). Effective recombination coefficients resulting from the three theories differ at low temperatures ($T \sim 100$K) where high n-shell collisions compete with radiative decay at densities where the system is not yet in local thermodynamic equilibrium. We have also explored the effect that the various l-changing theories have on the two-photon continuum spectrum of hydrogen in gaseous nebulae.

These theoretical predictions of the two-photon continuum could be compared with accurate observations of simple objects, with reliable temperature and density determinations, to determine which theory is correct. Astronomical observations are, at present, the only way to conduct this test and settle the question. This is not a

simple task, as homogeneous object lacking a small-scale structure is needed. The planetary nebula A39 described in Jacoby, Ferland & Korista (2001) is an example of it, however, it is too low in density. Finding suitable objects should be a high priority for future studies. We think these observations would be challenging, but would offer a unique test for new atomic physics.

REFERENCES

Baker J. G., Menzel D. H., 1938, ApJ, 88, 52
Brown R. L., Mathews W. G., 1970, ApJ, 160, 939
Chluba J., Ali-Haïmoud Y., 2016, MNRAS, 456, 3494
Chluba J., Sunyaev R. A., 2006, A&A, 446, 39
Chluba J., Vasil G. M., Dursi L. J., 2010, MNRAS, 407, 599
Fang X., Liu X.-W., 2011, MNRAS, 415, 181
Fang X., Liu X.-W., 2013, MNRAS, 429, 2791
Ferland G. J. et al., 2013, Rev. Mex. Astron. Astrofis., 49, 137
Ferland G. J., Henney W. J., O'Dell C. R., Peimbert M., 2016, Rev. Mex. Astron. Astrofis., 52, 261
Ferland G. et al., 2016, preprint (arXiv:1603.08902)
García-Rojas J., Esteban C., 2007, ApJ, 670, 457
Glover S. C. O., Chluba J., Furlanetto S. R., Pritchard J. R., Savin D. W., 2014, Adv. At. Mol. Opt. Phys., 63, 135
Guzmán F., Badnell N. R., Williams R. J. R., van Hoof P. A. M., Chatzikos M., Ferland G. J., 2016, MNRAS, 459, 3498 (P1)
Guzmán F., Badnell N. R., Williams R. J. R., van Hoof P. A. M., Chatzikos M., Ferland G. J., 2017, MNRAS, 464, 312 (P2)
Hummer D. G., Storey P. J., 1987, MNRAS, 224, 801
Irby V. D., Rolfes R. G., Makarov O. P., MacAdam K. B., Syrkin M. I., 1995, Phys. Rev. A, 52, 3809
Jacoby G. H., Ferland G. J., Korista K. T., 2001, ApJ, 560, 272
Jones D., Wesson R., García-Rojas J., Corradi R. L. M., Boffin H. M. J., 2016, MNRAS, 455, 3263
Liu X., 2012, in Manchado A., Stanghellini L., Schönberner D., eds, Proc. IAU Symp. 283, Atomic Processes in Planetary Nebulae. Kluwer, Dordrecht, p. 131
Liu X.-W., Storey P. J., Barlow M. J., Danziger I. J., Cohen M., Bryce M., 2000, MNRAS, 312, 585
MacAdam K. B., Crosby D. A., Rolfes R., 1980, Phys. Rev. Lett., 44, 980
MacAdam K. B., Rolfes R., Crosby D. A., 1981, Phys. Rev. A, 24, 1286
MacAdam K. B., Rolfes R. G., Sun X., Singh J., Fuqua W. L., III, Smith D. B., 1987, Phys. Rev. A, 36, 4254
McNabb I. A., Fang X., Liu X.-W., Bastin R. J., Storey P. J., 2013, MNRAS, 428, 3443
Nussbaumer H., Schmutz W., 1984, A&A, 138, 495
Osterbrock D. E., Ferland G. J., 2006, Astrophysics of Gaseous Nebulae and Active Galactic Nuclei, 2nd edn. University Science Books, Sausalito, CA
Peimbert M., 1967, ApJ, 150, 825
Peimbert A., Peimbert M., 2013, ApJ, 778, 89
Pengelly R. M., 1964, MNRAS, 127, 145
Pengelly R. M., Seaton M. J., 1964, MNRAS, 127, 165
Péquignot D., 1986, in Pequignot D., ed., Model Nebulae Comparison of Photoionization and steady shock models. p. 363

Péquignot D. et al., 2001, in Ferland G., Savin D. W., eds, ASP Conf. Ser. Vol. 247, Spectroscopic Challenges of Photoionized Plasmas. Astron. Soc. Pac., San Francisco, p. 533

Planck Collaboration XIII, 2016, A&A, 594, A13

Porter R. L., Ferland G. J., MacAdam K. B., Storey P. J., 2009, MNRAS, 393, L36

Schirmer M., 2016, PASP, 128, 114001

Spitzer L., Jr, Greenstein J. L., 1951, ApJ, 114, 407

Storey P. J., Sochi T., 2015, MNRAS, 446, 1864

Sun X., MacAdam K. B., 1993, Phys. Rev. A, 47, 3913

Vrinceanu D., Flannery M. R., 2001, Phys. Rev. A, 63, 032701

Vrinceanu D., Onofrio R., Sadeghpour H. R., 2012, ApJ, 747, 56

Zhang Y., Liu X.-W., 2002, MNRAS, 337, 499

This paper has been typeset from a TeX/LaTeX file prepared by the author.